Cloud optical thickness and effective particle radius derived from transmitted solar radiation measurements: Comparison with cloud radar observations

Nobuhiro Kikuchi,[1] Teruyuki Nakajima,[2] Hiroshi Kumagai,[1] Hiroshi Kuroiwa,[1] Akihide Kamei,[3] Ryosuke Nakamura,[4] and Takashi Y. Nakajima[5]

Received 14 June 2005; revised 17 November 2005; accepted 4 January 2006; published 5 April 2006.

[1] A method is presented for determining the optical thickness and effective particle radius of stratiform clouds containing liquid water drops in the absence of drizzle from transmitted solar radiation measurements. The procedure compares measurements of the cloud transmittance from the ground at water-absorbing and nonabsorbing wavelengths with lookup tables of the transmittance precomputed for plane-parallel, vertically homogeneous clouds. The optical thickness derived from the cloud transmittance may be used to retrieve vertical profiles of cloud microphysics in combination with the radar reflectivity factor. To do this, we also present an algorithm for solving the radar equation with a constraint of the optical thickness at the visible wavelength. Observations of clouds were made in August and September 2003 at Koganei, Tokyo, Japan, using a PREDE i-skyradiometer and a 95-GHz cloud radar Super Polarimetric Ice Crystal Detection and Explication Radar (SPIDER). The optical thickness and effective radius of water clouds were derived from the i-skyradiometer. Then, the vertical profile of the effective radius was retrieved from SPIDER, using the optical thickness determined from the i-skyradiometer. We found that the effective radii derived by using these two instruments were in good agreement.

Citation: Kikuchi, N., T. Nakajima, H. Kumagai, H. Kuroiwa, A. Kamei, R. Nakamura, and T. Y. Nakajima (2006), Cloud optical thickness and effective particle radius derived from transmitted solar radiation measurements: Comparison with cloud radar observations, *J. Geophys. Res.*, *111*, D07205, doi:10.1029/2005JD006363.

1. Introduction

[2] It is commonly accepted that the cloud radiative effect is one of the most uncertain factors for the projection of future global warming. The cloud optical thickness and effective particle radius are the key parameters which determine radiative properties of clouds such as reflection, transmission, and absorption of the solar radiation. So far, several methods to remotely sense these parameters have been proposed, in which the solar radiation reflected by clouds is measured at visible and near-infrared wavelengths from aircrafts or satellites [*Hansen and Pollack*, 1970; *Twomey and Seton*, 1980; *Twomey and Cocks*, 1982; *Curran and Wu*, 1982; *Nakajima and King*, 1990; *Nakajima and Nakajima*, 1995].

[3] The cloud optical thickness and effective radius may also be inferred from ground-based measurements of the transmitted solar radiation by a multispectral radiometer. Although ground-based observations of clouds cannot cover wide area as in aircraft or satellite observations, it is possible to make long-term monitoring of cloud radiative properties at a fixed observation site. In section 2 we describe a method to determine the optical thickness and effective radius of clouds containing liquid droplets in the absence of drizzle from spectral measurements of the cloud transmittance in the near infrared.

[4] In deriving the cloud optical thickness and effective radius from reflected or transmitted solar radiation measurements, clouds are usually assumed to be vertically homogeneous. In reality, however, water clouds are vertically inhomogeneous. We therefore need to examine how the vertical inhomogeneity affects the retrieval of the cloud parameters.

[5] To address this issue, 95-GHz cloud radar observations were also made. Vertical profiles of water clouds can be retrieved from the radar reflectivity factor if the liquid water path is given from a microwave radiometer [*Kumagai*

[1]National Institute of Information and Communications Technology, Tokyo, Japan.
[2]Center for Climate System Research, University of Tokyo, Chiba, Japan.
[3]National Institute for Environmental Studies, Ibaraki, Japan.
[4]National Institute of Advanced Industrial Science and Technology, Ibaraki, Japan.
[5]Department of Network and Computer Engineering, School of Engineering II, Tokai University, Tokyo, Japan.

0148-0227/06/2005JD006363$09.00

Table 1. Wavelengths of i-Skyradiometer Observations

	1	2	3	4	5	6	7	8	9	10	11
Wavelength, μm	0.315	0.34	0.38	0.4	0.5	0.675	0.87	0.94	1.02	1.6	2.2
FWHM, μm	-	-	-	-	-	-	-	-	0.01	0.02	0.02

et al., 2000], or the optical thickness at the visible wavelength is given by a visible/near-infrared radiometer [*Austin and Stephens*, 2001]. In section 3 we describe our algorithm for solving the radar equation with a constraint of cloud optical thickness at visible wavelength, by which we can derive vertical profiles of cloud microphysics. The results of our observations are presented in section 4.

2. Optical Thickness and Effective Radius Derived From Cloud Transmittance Measurements

2.1. Cloud Transmittance

[6] Let us consider the solar radiation incident on a plane-parallel atmosphere. We express the diffusely reflected radiation at the top of the atmosphere and the diffusely transmitted radiation at the bottom of the atmosphere as $I(0, -\mu, \phi)$ and $I(\tau_c, \mu, \phi)$, respectively. The reflection function $R(\tau_c; \mu, \mu_0, \phi)$ and the transmission function $T(\tau_c; \mu, \mu_0, \phi)$ are then defined, respectively, by

$$R(\tau_c; \mu, \mu_0, \phi) = \frac{\pi I(0, -\mu, \phi)}{\mu_0 F_0} \tag{1}$$

$$T(\tau_c; \mu, \mu_0, \phi) = \frac{\pi I(\tau_c, \mu, \phi)}{\mu_0 F_0}. \tag{2}$$

[7] In these expressions, τ_c is the optical thickness of the cloud, μ is the absolute value of the cosine of the observation angle measured with respect to the positive τ_c direction, ϕ is the relative azimuth angle between the direction of propagation of the emerging radiation and the incident solar direction, μ_0 is the cosine of the solar zenith angle θ_0, and F_0 is the incident solar flux density. The cloud optical thickness is defined at the wavelength 0.5 μm throughout this paper.

[8] *Nakajima and King* [1990] described a method, as well as its underlying physics, for deriving the optical thickness and effective radius of clouds from measurements of the reflection function $R(\tau_c; \mu, \mu_0, \phi)$. On the other hand, this paper deals with the transmission function measured from the ground viewing zenith, that is, $\mu = 1$. We therefore do not need to consider the dependence of the transmission function on ϕ, and we will use the term 'transmittance' for $T(\tau_c; \mu, \mu_0, \phi)$ with $\mu = 1$.

[9] For a cloud particle size distribution $n(r)$, we adopt a lognormal distribution of the form

$$n(r) = \frac{N}{\sqrt{2\pi}\sigma r} \exp\left[-\frac{(\ln r - \ln r_0)^2}{2\sigma^2}\right], \tag{3}$$

where N is the total number concentration, r_0 is the mode radius, and σ is the standard deviation. In terms of these parameters, the effective radius, defined by

$$r_e = \int_0^\infty r^3 n(r) dr \Big/ \int_0^\infty r^2 n(r) dr, \tag{4}$$

is expressed as

$$r_e = r_0 \exp(5\sigma^2/2). \tag{5}$$

Following *Nakajima and King* [1990], we adopted $\sigma = 0.35$.

[10] In determining simultaneously the cloud optical thickness and effective radius from reflection or transmission function measurements, it is essential to adopt both water-absorbing and nonabsorbing wavelengths. At water-absorbing wavelengths, water droplets absorb more solar radiation as the particles increase in size, whereas at nonabsorbing wavelength, water droplets absorb little solar radiation. In this paper we discuss cloud transmission properties for three near-infrared wavelengths at 1.02, 1.6, and 2.2 μm. Among these wavelengths, 1.02 μm has been adopted as a nonabsorbing wavelength, while the other two are water-absorbing wavelengths. These three wavelengths correspond to channels 9, 10, and 11 of a Sun-sky scanning photometer called i-skyradiometer, manufactured by PREDE Co. Ltd. (product name POM02), as summarized in Table 1.

[11] We computed the transmittance for various values of the cloud optical thickness and effective radius using rstar-4b, an atmospheric radiative transfer code based on the discrete ordinate method [*Nakajima and Tanaka*, 1986, 1988; *Stamnes et al.*, 1988; http://www.ccsr.u-tokyo.ac.jp/~clastr/Datap.html). The US standard atmosphere model was adopted to simulate the transmitted solar radiation observed from the ground. A cloud layer with geometrical thickness 1 km is inserted into 1–2 km altitude for water clouds, or 5–6 km altitude for ice clouds. Water vapor is assumed to be saturated in the cloud layer. The underlying surface is assumed to be a Lambert surface with flux albedo A_g. The measured filter response function was found to be well approximated for channels 9, 10, and 11 of the i-skyradiometer used in this paper as

$$f(x) = \exp\left(-\ln 2|4x|^4\right), \tag{6}$$

where x is wavelength in unit of 2× FWHM listed in Table 1. The numerical results of the transmittance presented below were obtained by convolving the monochromatic radiance with the filter response function as expressed by equation (6) in the range $-0.5 \le x \le 0.5$.

[12] In the present study we apply our retrieval method to water clouds. The transmittance of ice clouds are computed assuming that the ice particles are spherical. Although this approximation is not sufficient for retrieving microphysical properties of ice clouds, it would be adequate to discriminate between water and ice clouds from spectral measurements of the cloud transmittance [*Curran and Wu*, 1982].

[13] In this subsection we examine the transmittance of a cloudy atmosphere over a nonreflecting surface, and effects of surface reflection will be discussed in the next subsection. Figure 1 illustrates the transmittance at a nonabsorbing

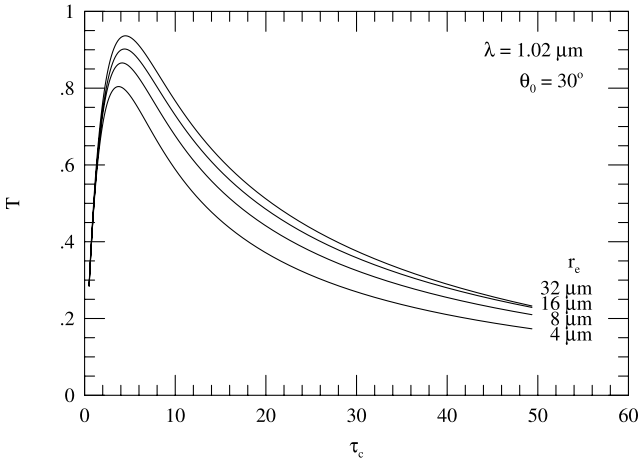

Figure 1. Cloud transmittance at 1.02 μm as a function of cloud optical thickness for four values of effective radius. Results apply to water clouds when the solar zenith angle $\theta_0 = 30°$.

wavelength 1.02 μm as a function of τ_c for several values of r_e. These numerical results were computed for water clouds assuming the solar zenith angle $\theta_0 = 30°$. In general, for a fixed value of r_e, the transmittance decreases with increasing τ_c if the cloud optical thickness is sufficiently large. Also, the transmittance approaches zero in the limit of zero optical thickness. Thus there should be a value of τ_c at which the transmittance takes its maximum value. Figure 1 shows that the value of τ_c which maximizes the transmittance lie in the range $4 < \tau_c < 5$ and increases slightly with increasing r_e. This behavior of the transmittance indicates that every measured value of the transmittance has two corresponding values of τ_c. In other words, even if the effective radius is known or assumed, cloud optical thickness cannot be determined uniquely from the transmittance at a nonabsorbing channel. This makes the retrieval method using the transmittance somewhat more complicated than that using the reflection function, which is a monotonically increasing function of τ_c.

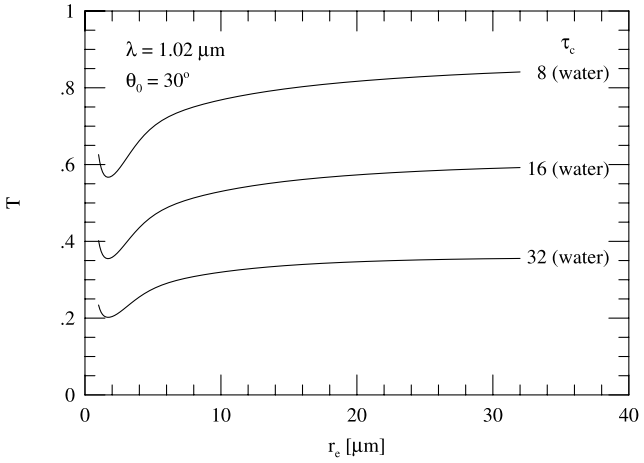

Figure 2. Cloud transmittance at 1.02 μm as a function of effective radius for three values of cloud optical thickness. Results apply to water clouds when the solar zenith angle $\theta_0 = 30°$.

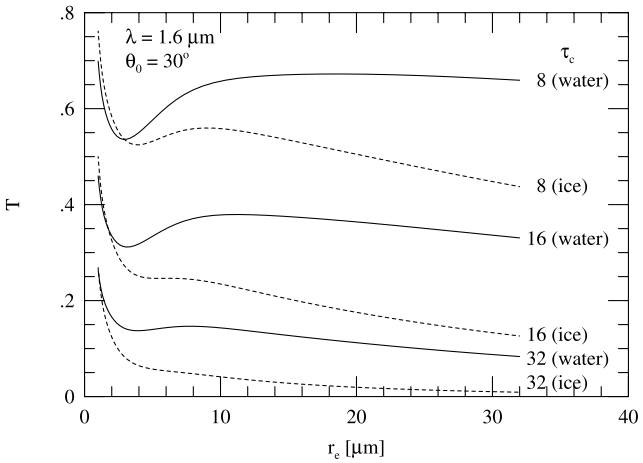

Figure 3. Cloud transmittance at 1.6 μm as a function of effective radius for three values of cloud optical thickness. Results apply to water clouds (solid curves) and ice clouds (dashed curves) when the solar zenith angle $\theta_0 = 30°$.

[14] Another important feature seen in Figure 1 is that the transmittance at 1.02 μm increases with increasing r_e. For more detailed examination, we plot in Figure 2 the transmittance at 1.02 μm as a function of the effective radius for $\tau_c = 8$, 16 and 32. Figure 2 shows that the local minimum of the transmittance occurs at about $r_e \simeq 2$ μm and that the transmittance increases monotonically as r_e increases when $r_e > 2$ μm. On the other hand, dependence of the transmittance on the effective radius is found to be more complicated at water-absorbing wavelengths. Figure 3 illustrates the transmittance at 1.6 μm as a function of the effective radius both for water clouds (solid curves) and for ice clouds (dashed curves). It can be seen in Figure 3 that the transmittance at 1.6 μm has both the local minimum and maximum, which become more pronounced as τ_c increases. At sufficiently large effective radius, the transmittance declines with increasing r_e. Similar results have been obtained for the transmittance at 2.2 μm as shown in Figure 4. It is also found from Figures 2–4 that the position of the local minimum increases as wavelength increases.

[15] The sensitivity of the transmittance to the effective radius presented in Figures 2–4 can be understood from

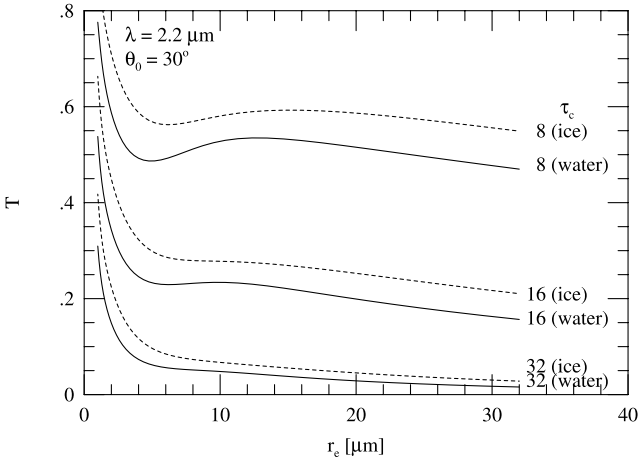

Figure 4. As in Figure 3 but for wavelength at 2.2 μm.

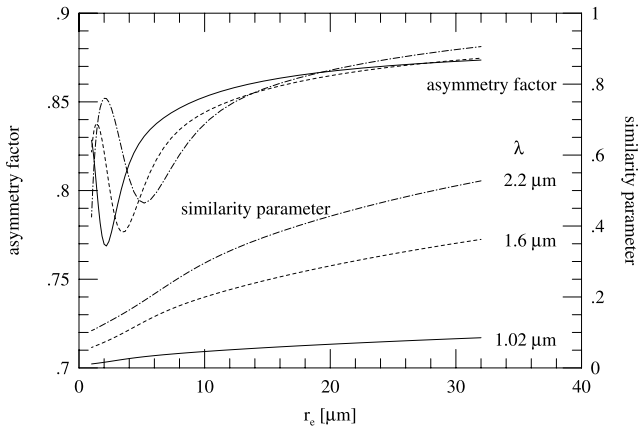

Figure 5. Asymmetry factors and similarity parameters as a function of effective radius of water droplets for wavelengths at 1.02, 1.6, and 2.2 μm.

Figure 5, which shows the asymmetry factor g and similarity parameter s, as defined by

$$s = \left(\frac{1-\omega_0}{1-\omega_0 g}\right)^{1/2}, \tag{7}$$

as a function of the effective radius. Here ω_0 is the single scattering albedo, and the results shown in Figure 5 were computed for water droplets at wavelengths 1.02, 1.6 and 2.2 μm. Figure 5 shows that the local minimum of the asymmetry factor occurs for effective radius between 2 μm and 5 μm depending on wavelength. The positions of the local minimum of the asymmetry factor is consistent with those of the transmittance presented in Figures 2–4. Therefore it is concluded that the local minimum of the transmittance occurs for effective radius at which scaled optical thickness τ'_c, defined by

$$\tau'_c = (1-g)\tau_c, \tag{8}$$

takes its local maximum value. Figure 5 also shows that once the asymmetry factor attained its local minimum value, it increases monotonically with increasing effective radius. Thus the increase of the transmittance at 1.02 μm with increasing effective radius for $r_e > 2$ μm is a result of decreasing scaled optical thickness. At water-absorbing wavelengths, however, absorption becomes progressively effective as the effective radius increases as shown in Figure 5. As a result, the transmittance at 1.6 and 2.2 μm declines for sufficiently large effective radius, as illustrated Figures 3 and 4.

[16] It is worth noting that at 1.6 μm the transmittance of water clouds is almost always larger than that of ice clouds, while at 2.2 μm the transmittance of water clouds is always smaller than that of ice clouds. Furthermore, the difference in transmittance between water and ice at 1.6 μm is greater than the difference at 2.2 μm. The degree to which the transmittance for water and ice differ at these two wavelengths is a direct consequence of the difference in refractive indices of water and ice. Therefore simultaneous measurements of the transmittance at 1.6 and 2.2 μm can be used to infer cloud thermodynamic phase [*Curran and Wu*, 1982].

2.2. Effects of Surface Reflection

[17] Assuming that the surface underlying a cloud reflects transmitted solar radiation according to Lambert's law with flux albedo A_g, we examine effects of surface reflection on the transmittance. Figure 6 illustrates the transmittance at 1.02 μm as a function of optical thickness for clouds overlying a Lambert surface with four different values of the flux albedo (A_g = 0.0, 0.2, 0.4 and 0.6). These results were computed for water clouds with r_e = 8 μm when the solar zenith angle $\theta_0 = 30°$. In Figure 7 the transmittance at 1.6 and 2.2 μm is shown as a function of effective radius and the flux albedo. In computing the transmittance shown in Figure 7, we assumed $\tau_c = 16$ and $\theta_0 = 30°$.

[18] It can be seen from Figures 6 and 7 that the influence of surface reflection decreases as wavelength increases. This is a result of increasing absorption of solar radiation by

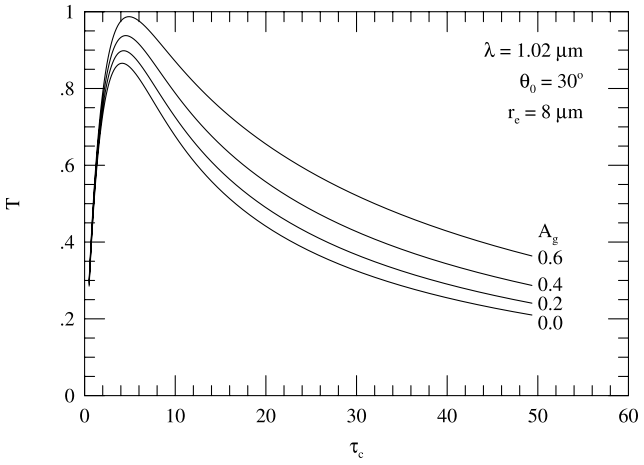

Figure 6. Cloud transmittance at 1.02 μm as a function of cloud optical thickness for various values of ground albedo A_g. Results apply to water clouds with effective radius r_e = 8 μm when the solar zenith angle $\theta_0 = 30°$.

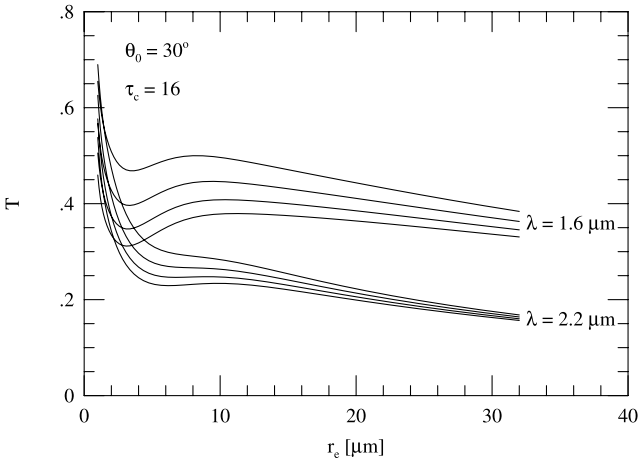

Figure 7. Cloud transmittance at 1.6 and 2.2 μm as a function of effective radius for various values of ground albedo A_g. Results apply to water clouds with optical thickness $\tau_c = 16$ when the solar zenith angle $\theta_0 = 30°$.

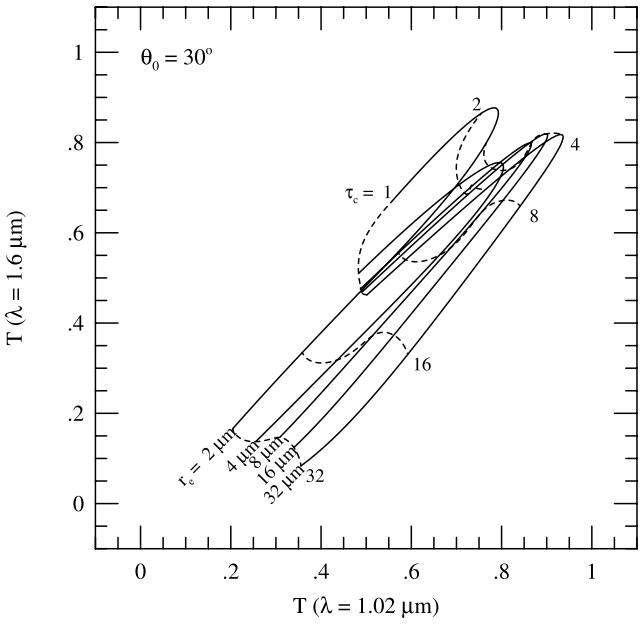

Figure 8. Computed relationships between the cloud transmittance at 1.02 and 1.6 μm for various values of the cloud optical thickness and effective radius for the case $\theta_0 = 30°$.

cloud droplets. However, the influence of surface reflection cannot be neglected for all possible ranges of cloud optical thickness and effective radius. Therefore the surface reflectance needs to be assumed accurately for successful retrievals of cloud microphysical properties from transmitted solar radiation measurements.

2.3. Determination of Optical Thickness and Effective Radius

[19] The principles of the simultaneous determination of τ_c and r_e are demonstrated in Figure 8, where computed relationships between the transmittance at 1.02 and 1.6 μm are shown for water clouds when the solar zenith angle $\theta_0 = 30°$ and the flux albedo $A_g = 0$ at both wavelengths. The dashed curves in Figure 8 represent the transmittance that result for specified values of τ_c, whereas the solid curves represent the transmittance that result for specified values of r_e. Solutions for τ_c and r_e can be determined from transmittance measurements at the two wavelength, if cloud thermodynamic phase is known a priori, and if the surface reflectance is known at each wavelength.

[20] However, the cloud thermodynamic phase is not known a priori unless additional observational information is available. Moreover, it can be seen from Figure 8 that multiple solutions of τ_c and r_e are possible in some cases. Therefore measurements of the transmittance at 1.02 and 1.6 μm alone will not suffice to unambiguously determine τ_c and r_e. This ambiguity will be reduced by adopting an additional measurement at 2.2 μm. Figure 9 is similar to Figure 8, but for computed relationships between the transmittance at 1.02 and 2.2 μm. If the cloud we now observe is actually a water cloud, and if we use lookup tables computed for water clouds, then almost same values of τ_c and r_e should be derived from analysis using either 1.6 μm or 2.2 μm. On the other hand, the cloud is composed of ice particles, we will get better agreement between 1.6 μm and 2.2 μm from lookup tables computed for ice clouds. The cloud thermodynamic phase is thus determined. An appropriate solution may also be selected from multiple ones in the same fashion.

[21] We note that comparing Figure 8 with Figure 9, it is clear that the transmittance is more sensitive to effective radius at 2.2 μm than at 1.6 μm. This suggests that effective radius may be determined more accurately by the 2.2 μm channel than by the 1.6 μm channel if the same measurement accuracy can be achieved for both channels.

[22] Although the cloud transmittance presented in Figures 8 and 9 was computed assuming $A_g = 0$ at all channels, we need to specify proper values of A_g in retrieving τ_c and r_e from observations. We therefore examine sensitivity of the retrieval to the uncertainties in the surface albedo as follows: We computed lookup tables of the cloud transmittance assuming the flux albedo $A_g = 0.18$, 0.14 and 0.11 for channels 9, 10 and 11 of the i-sky-radiometer, respectively. Then, we computed the transmittance of a water cloud with some known values of τ_c and r_e over the ground whose flux albedo was randomly perturbed around the assumed value. The cloud transmittance computed in this way was then inverted to the optical thickness and effective radius, which, in general, differ from the true values of τ_c and r_e because of the perturbed flux albedo. From 10^3 trials, we estimated maximum errors in retrieving optical thickness $E\tau_c$ and effective radius E_{re} which result from 10% uncertainty in the flux albedo. The results are tabulated in Table 2 for two combinations of τ_c and r_e. We find that if the 2.2 μm channel is used in the retrieval, τ_c can be determined with errors less than 1%, whereas 8% errors would be introduced in the retrieval of r_e. It is also found that the 2.2 μm channel introduces smaller retrieval errors than the 1.6 μm channel, because the cloud transmittance is less sensitive to the surface reflectance at 2.2 μm than 1.6 μm as demonstrated in Figure 7.

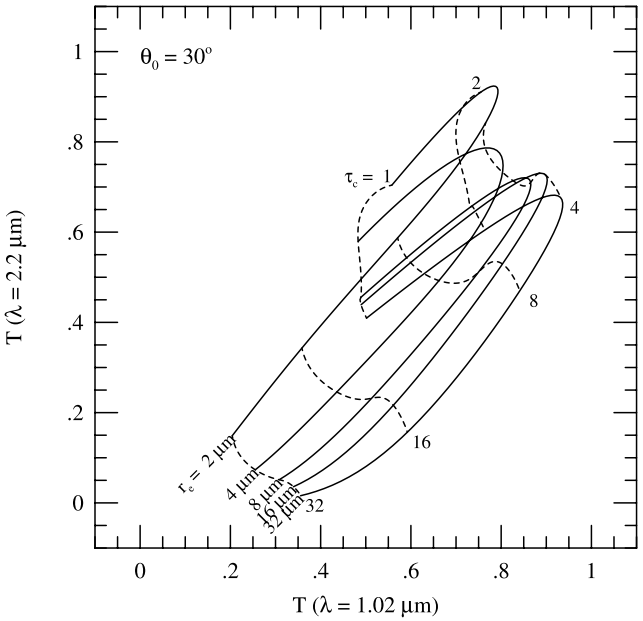

Figure 9. As in Figure 8 but for the cloud transmittance at 1.02 and 2.2 μm.

Table 2. Percent Errors Associated With 10% Uncertainty of the Surface Albedo in the Retrieval of the Cloud Optical Thickness ($E(\tau_c)$) and Effective Radius ($E(r_e)$)

		1.02 + 1.6 μm		1.02 + 2.2 μm	
τ_c	r_e, μm	$E(\tau_c)$	$E(r_e)$	$E(\tau_c)$	$E(r_e)$
16	4	2.1	8.0	0.7	2.5
16	8	5.0	21.9	0.5	8.2

[23] Our method for determining τ_c and r_e from transmitted solar radiation measurements have several similarities with the solar reflection method described by *Nakajima and King* [1990]. Both methods use water-absorbing and nonabsorbing wavelengths. The cloud transmission/reflection properties at these wavelengths, which form the basis of the algorithms, can be understood qualitatively in terms of the scaled optical thickness and the similarity parameter. The solar reflection method is applied to aircraft or satellite observations to determine cloud microphysical properties in wide area, whereas the solar transmission method described in this paper will be suited to long-term monitoring of cloud microphysics at fixed observation sites.

3. Cloud Vertical Profiles Derived From Radar Observations

[24] In this section we describe an algorithm which can be used to derive vertical structure of cloud microphysics from radar reflectivity factor in combination with cloud optical thickness at visible wavelength. In this algorithm it is assumed that the cloud droplet number concentration is constant with height. Although this assumption is reasonable for water clouds without drizzle, this is not the case for drizzle and ice clouds. Therefore the algorithm described in this section can be applied only to water clouds without drizzle.

[25] The radar signal $P(R)$ from the range R may be written in the unit of power as

$$P(R) = \frac{C}{R^2} Z_e(R) \exp\left[-2\int_0^R \sigma_{\text{ext}}(R')dR'\right], \tag{9}$$

where C is the calibration constant including instrument parameters, Z_e is the effective reflectivity, and σ_{ext} is the extinction coefficient. For a cloud with particle size distribution $n(r)$, Z_e and σ_{ext} are expressed as

$$Z_e = \frac{\lambda^4}{\pi^5 |K|^2}\left[\int_0^\infty C_{\text{back}}(r) n(r) dr\right] \tag{10}$$

and

$$\sigma_{\text{ext}} = \int_0^\infty C_{\text{ext}}(r) n(r) dr, \tag{11}$$

where λ is the radar wavelength, K is defined using complex refractive index of water m as $K = (m^2 - 1)/(m^2 + 2)$, and $C_{\text{back}}(r)$ and $C_{\text{ext}}(r)$ are the backscattering and extinction cross sections of a particle with radius r, respectively.

[26] We consider a radar system with range resolution ΔR. The radar signal from ith range centered at $R = R_i$ may be obtained by averaging equation (9) over ΔR as

$$P_i = \frac{1}{\Delta R}\int_{R_{i-1/2}}^{R_{i+1/2}} P(R) dR, \tag{12}$$

where $R_{i\pm1/2} = R_i \pm 1/2\Delta R$. We assume that cloud microphysical properties are piecewisely constant, that is, in $R_{i-1/2} \le R \le R_{i+1/2}$,

$$Z_e(R) = Z_i \tag{13}$$

$$\sigma_{\text{ext}}(R) = \sigma_i. \tag{14}$$

Assuming $\Delta R \ll R$, equation (12) leads to

$$P_i = \frac{C}{R^2} Z_i^{\text{obs}}, \tag{15}$$

where Z_i^{obs} corresponds to the observed radar reflectivity factor, and is defined as

$$Z_i^{\text{obs}} = Z_i \exp\left[-2\tau_{i-1/2}\right] \frac{1 - \exp[-2\sigma_i \Delta R]}{2\sigma_i \Delta R}. \tag{16}$$

In this expression, $\tau_{i-1/2}$ is the optical depth up to $R = R_{i-1/2}$, that is,

$$\tau_{i-1/2} = \int_0^{R_{i-1/2}} \sigma_{\text{ext}}(R) dR. \tag{17}$$

The optical depth $\tau_{i-1/2}$ is defined at the radar wavelength, and should not be confused with the cloud optical thickness τ_c.

[27] *Okamoto et al.* [2003] developed a forward-type algorithm for solving the averaged radar and lidar equations. Here, we take somewhat different approach to solve the averaged radar equation (15) with a constraint of the optical thickness at the visible wavelength. We first define the following quantity:

$$\gamma_i \equiv Z_i \frac{1 - \exp[-2\sigma_i \Delta R]}{2\sigma_i \Delta R}. \tag{18}$$

Note that γ_i is a function of liquid water content and effective radius in the ith range. Taking a ratio of the observed reflectivity factor in ith and $(i + 1)$th ranges, we have

$$\frac{Z_i^{\text{obs}}}{Z_{i+1}^{\text{obs}}} = \frac{\gamma_i}{\gamma_{i+1}} \frac{\exp\left[-2\tau_{i-1/2}\right]}{\exp\left[-2\tau_{i+1/2}\right]} = \frac{\gamma_i}{\gamma_{i+1}} \exp[2\sigma_i \Delta R]. \tag{19}$$

In deriving the expression (19), we have used the relation $\tau_{i+1/2} - \tau_{i-1/2} = \sigma_i \Delta R$.

[28] We denote the liquid water content of ith range by ρ_i. Then the effective reflectivity factor and extinction coefficient can be written as

$$Z_i = \rho_i \zeta_i(r_e) \tag{20}$$

$$\sigma_i = \rho_i \kappa_i(r_e), \tag{21}$$

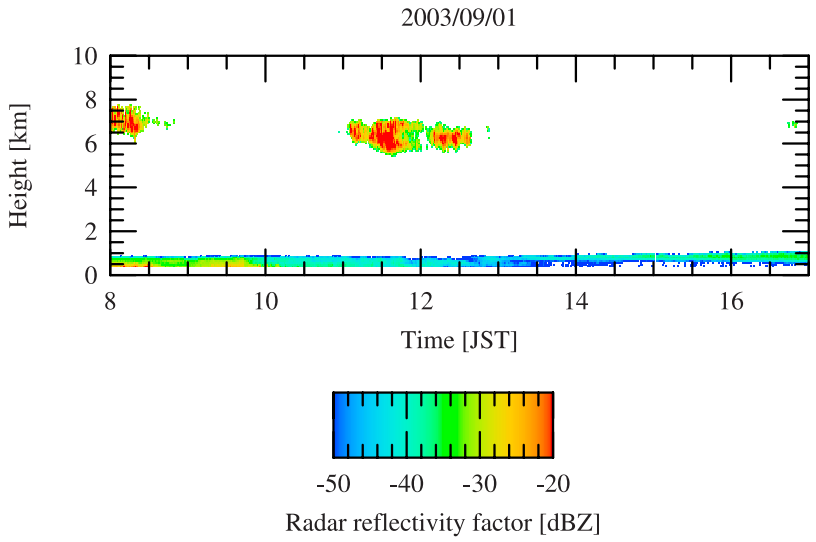

Figure 10. Observed radar reflectivity for 1 September 2003 at Koganei, Tokyo.

where ζ_i is the effective reflectivity factor per unit mass, and κ_i is the mass extinction coefficient. Both ζ_i and κ_i are functions of the effective radius of the ith range. Using expressions (18), (20) and (21) in equation (19), ρ_i can be written as

$$\rho_i(r_e) = \frac{1}{2\kappa_i(r_e)\Delta R} \times \ln\left[1 + \frac{2\kappa_i(r_e)\Delta R}{\zeta_i(r_e)} \frac{Z_i^{\mathrm{obs}}}{Z_{i+1}^{\mathrm{obs}}} \gamma_{i+1}\right]. \quad (22)$$

Another expression of liquid water content is given by integrating equation (3) as

$$\rho_i(r_e) = N\rho_w \frac{4}{3}\pi r_e^3 \exp\left[-3\sigma^2\right], \quad (23)$$

where ρ_w is the density of liquid water. We assume that N is constant along vertical direction.

[29] Equating (22) and (23), we obtain

$$\frac{1}{2\kappa_i(r_e)\Delta R} \ln\left[1 + \frac{2\kappa_i(r_e)\Delta R}{\zeta_i(r_e)} \frac{Z_i^{\mathrm{obs}}}{Z_{i+1}^{\mathrm{obs}}} \gamma_{i+1}\right] = N\rho_w \frac{4}{3}\pi r_e^3 \exp\left[-3\sigma^2\right]. \quad (24)$$

[30] Suppose that the liquid water content and effective radius in the $(i + 1)$th range are known. Then γ_{i+1} appearing in equation (24) can be calculated from equation (18). Since Z_i^{obs} and Z_{i+1}^{obs} are known from observations, equation (24) can be solved for r_e in the ith range. Once r_e is determined,

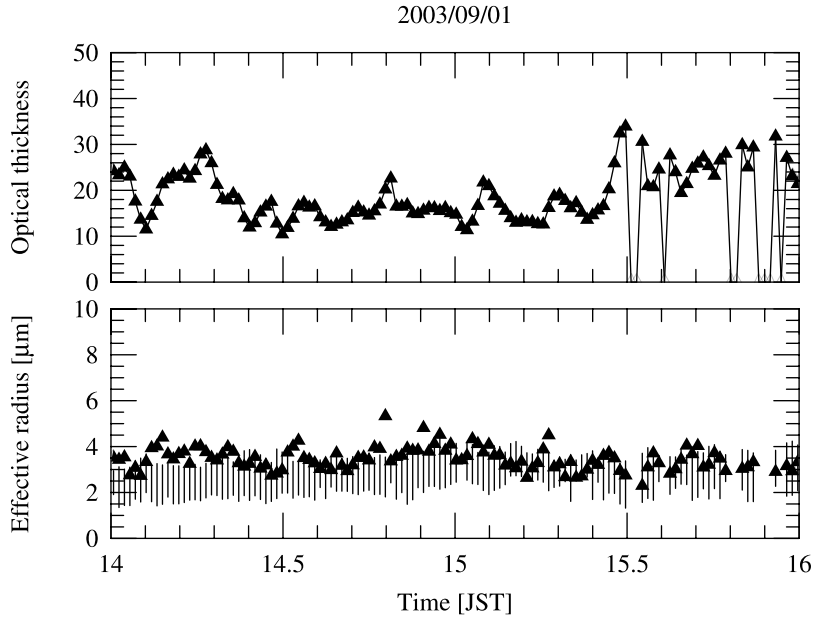

Figure 11. Cloud microphysical properties for 1 September 2003: (top) cloud optical thickness and (bottom) effective radius derived from i-skyradiometer (solid triangles). Also shown is the range of effective radius along the vertical direction derived by SPIDER with constraint of cloud optical thickness obtained by i-skyradiometer (vertical bars).

ρ_i is calculated from equation (22) or (23). This procedure defines a backward algorithm for determination of the liquid water content and effective radius.

[31] With initial guess for N and for ρ and r_e in the nth range, ρ and r_e can be determined from $i = n - 1$ to $i = 1$. Then we can calculate cloud optical thickness at the visible wavelength, which we denote by τ'_c. The value of τ'_c might be different from the correct value of the cloud optical thickness. We then update N according to

$$N \rightarrow N \frac{\tau_c}{\tau'_c} \tag{25}$$

and iterate the above procedure until τ'_c converges to τ_c.

[32] In our backward algorithm, we need ρ and r_e in nth range. We determine these values as follows. We rewrite equation (16) for nth range as

$$Z_n^{\mathrm{obs}} = Z_n \exp\left[-2\tau_{n+1/2}\right] \frac{\exp[2\sigma_n \Delta R] - 1}{2\sigma_n \Delta R}, \tag{26}$$

where $\tau_{n+1/2}$ corresponds to the optical thickness at the radar wavelength. After rearranging equation (26), we obtain

$$\rho_n(r_e) = \frac{1}{2\kappa_n(r_e)\Delta R} \times \ln\left[1 + \frac{2\kappa_n(r_e)\Delta R}{\zeta_n(r_e)} Z_n^{\mathrm{obs}} \exp\left[\tau_{n+1/2}\right]\right]. \tag{27}$$

Equating (23) and (27), we obtain ρ and r_e for nth layer, with N and $\tau_{n+1/2}$ calculated from the previous iteration.

[33] We need an initial guess for N and $\tau_{n+1/2}$ when we start the iteration procedure. We can set $\tau_{n+1/2} = 0$ as an initial guess, because clouds are not so optically thick at the radar wavelength. With an initial guess of r_e (for example, r_e = 10 μm), equation (27) gives ρ_n, which, in combination with equation (23), gives initial guess for N.

4. Results

[34] Ground-based observations of clouds were made in August and September 2003 at Koganei (35.71°N, 139.49°E), Tokyo, Japan. The instruments used were a PREDE i-skyradiometer and a 95-GHz cloud radar named Super Polarimetric Ice Crystal Detection and Explication Radar (SPIDER) [*Horie et al.*, 2000]. Figure 10 illustrates the time-height cross section of the radar reflectivity factor observed by SPIDER on 1 September. From these cloud radar data, the observation time from 14:00 to 16:00 JST was found to be suitable for the retrieval method presented in section 2, because the cloud in this period was a single-layer water cloud.

[35] Transmitted solar radiation was measured with about 1 minute interval at channels 9, 10 and 11 of the i-sky-radiometer. Radiometric calibration of these channels has been done using an integrating sphere maintained at Japan Aerospace Exploration Agency (JAXA). The observed radiance was converted to the transmittance as defined by equation (2), and then analyzed with the method described in section 2. To do this, however, we need to know the surface reflectance at wavelengths appropriate for the channels 9, 10 and 11. To estimate the surface reflectance, we decided to utilize satellite data. We searched for the minimum radiance values in channels 24 (1.05 μm), 28 (1.64 μm) and 29 (2.21 μm) of Global Imager (GLI) aboard ADEOS-II satellite observed over Koganei in August 2003. The minimum radiance values, which most likely arise under a clear sky condition, were then compared with the output of the GLI Signal Simulator for various values of ground surface albedo. The values of ground surface albedo which reproduced the observed minimum radiance were found to be 0.18, 0.14 and 0.11 for channels 24, 28 and 29 of GLI, respectively. These values were adopted as the flux albedo at channels 9, 10 and 11 of the i-skyradiometer. It is worth noting that the surface albedo can also be obtained from observations by the MODIS

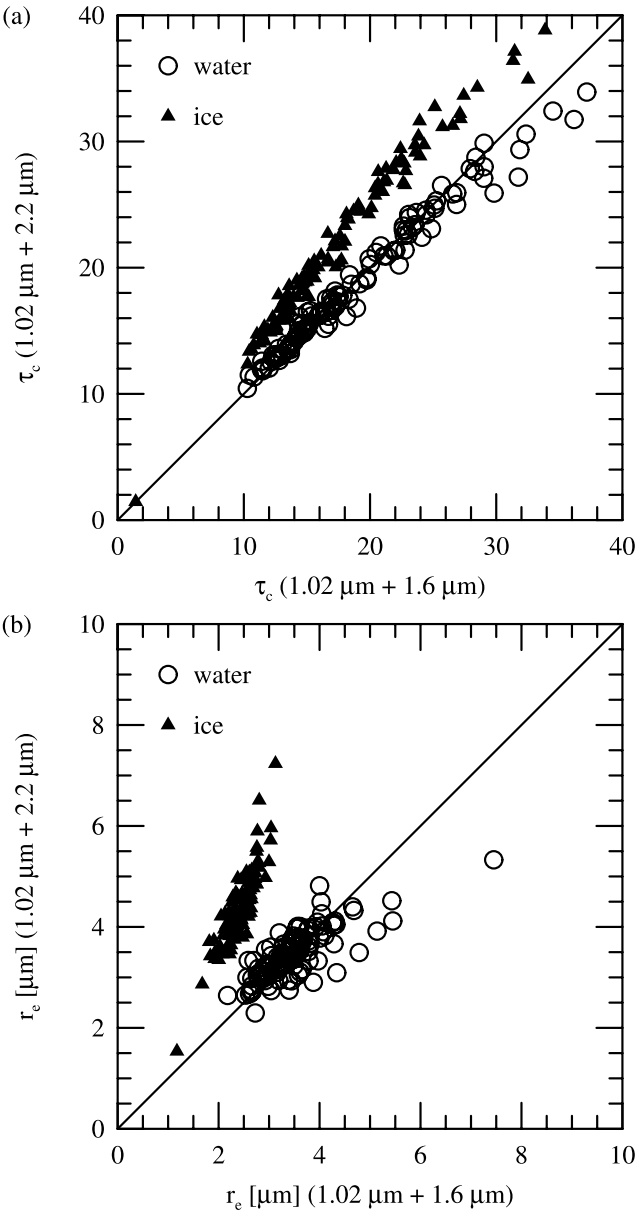

Figure 12. (a) Relationship between the optical thickness derived from the 1.6 μm channel and the 2.2 μm channel. Open circles represent τ_c derived using lookup tables for water clouds, whereas solid triangles represent τ_c derived from lookup tables for ice clouds. (b) As in Figure 12a but for the effective radius.

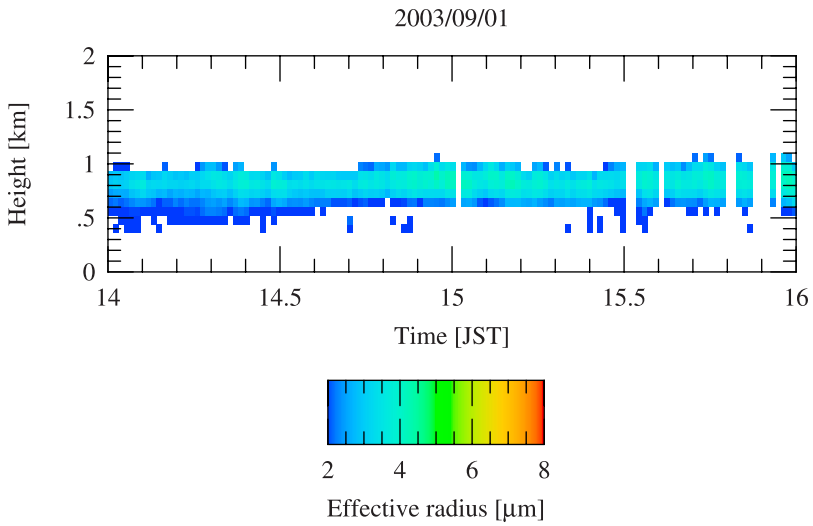

Figure 13. Effective particle radius for 1 September 2003 derived by SPIDER with constraint of cloud optical thickness obtained by i-skyradiometer.

instruments [*Moody et al.*, 2005], which may be used for many other ground-based observation sites.

[36] Figure 11 illustrates the cloud optical thickness (top) and effective radius (bottom) derived from measurements of the transmittance as described in section 2. It can be seen from Figure 11 that τ_c varies around 15, wheres r_e ranges from 3 μm to 5 μm. In a few cases τ_c is plotted as $\tau_c = 0$, which indicates that the cloud was so optically thick that the radiance at channel 11 (2.2 μm) of the i-skyradiometer was below the detection limit.

[37] The results presented in Figure 11 were determined by the transmittance at 1.02 μm and 2.2 μm. As described in section 2, independent estimates of τ_c and r_e may also be obtained from the transmittance at 1.02 μm and 1.6 μm. In general, there are some differences between results obtained using the 1.6 μm channel and that obtained using the 2.2 μm channel.

[38] Figure 12a compares the optical thickness derived from these two different channels. Open circles represent the optical thickness derived from the lookup table computed for water clouds, whereas filled triangles represent the optical thickness derived from the lookup table computed for ice clouds. As denoted by open circles in Figure 12a, the optical thickness derived from the 1.6 μm channel well corresponds with that derived from the 2.2 μm channel if the lookup table computed for water clouds is adopted. On the other hand, if the lookup table computed for ice clouds is adopted, the optical thickness derived from the 2.2 μm channel is systematically larger than that derived from the 1.6 μm channel. Therefore the observed cloud may be considered as a water cloud, which is also evident from the cloud radar observation shown in Figure 10. The same conclusion may be obtained from Figure 12b, which compares the effective radius derived from the two different channels.

[39] The cloud optical thickness obtained from measurements of the transmittance may be used to derive vertical profiles of cloud microphysics in combination with radar reflectivity factor. Figure 13 shows the time-height cross section of the effective radius derived from the method described in section 3. Returning to bottom plot of Figure 11, the minimum and maximum values of the effective radius along the vertical direction are superimposed by vertical bars. In most cases, the effective radius derived from transmission function measurements lies in the range obtained from cloud radar observations.

[40] One might have a question whether it is justified to derive cloud vertical profiles from radar reflectivity factor by using the optical thickness obtained assuming that the cloud is vertically homogeneous. To address this issue, we examined how vertical inhomogeneity of clouds affects the optical thickness derived from measurements of the transmittance as follows. For a cloud with vertical distribution of the effective radius shown in Figure 13, we compute the transmittance at the channels 9, 10 and 11 of the i-skyradiometer using rstar-4b. This simulated transmittance is then analyzed by the method described in section 2, where vertical homogeneity is assumed, to obtain the optical thickness.

[41] In Figure 14 the percent error of the derived optical thickness is plotted against the true optical thickness of the

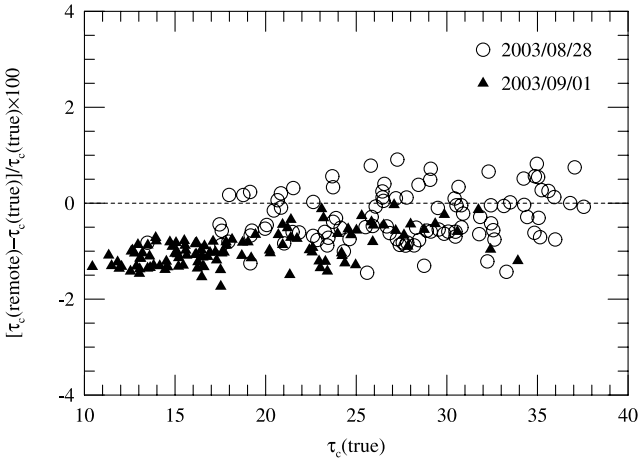

Figure 14. Relative differences between cloud optical thicknesses derived assuming vertically homogeneous or inhomogeneous cloud layers.

vertically inhomogeneous cloud. In addition to the data on 1 September, data observed on 28 August are also plotted in Figure 14. We find that the retrieval error associated with vertical inhomogeneity is within 2% for most cases. This result indicates that the cloud optical thickness can be derived accurately from measurements of the transmittance as described in section 2, even if the cloud layer is vertically inhomogeneous.

5. Conclusions

[42] We have developed an algorithm to derive the optical thickness and effective radius of stratiform water clouds from measurements of the transmitted solar radiation at the near-infrared from the ground. A method has also been introduced for deriving vertical profiles of water cloud microphysics from radar reflectivity factor, in which the cloud optical thickness at the visible wavelength is used as a constraint in solving the radar equation. We made ground-based observations of water clouds using an i-skyradiometer and a cloud radar SPIDER, and obtained good agreement between these two methods for the effective radius. Finally, we examined the effect of vertical inhomogeneity of clouds on the retrieval using measurements of the transmittance, and the error associated with vertical inhomogeneity was estimated to be <2%.

[43] **Acknowledgments.** The authors are grateful to Yasuji Yamamoto of JAXA for calibration of the i-skyradiometer using an integrating sphere. Tamio Takamura of Chiba University and Kazuma Aoki of Toyama University, who manage the SKYNET project, are also acknowledged. This work was supported by the JAXA/ADEOS-II/GLI project and ESA-JAXA-NiCT joint project of the EarthCARE satellite mission.

References

Austin, R. T., and G. L. Stephens (2001), Retrieval of stratus cloud microphysical parameters using millimeter-wave radar and visible optical depth in preparation for CloudSat, *J. Geophys. Res.*, *106*, 28,233–28,242.

Curran, R. J., and M. L. C. Wu (1982), Skylab near-infrared observations of clouds indicating supercooled liquid water droplets, *J. Atmos. Sci.*, *39*, 635–647.

Hansen, J. E., and J. B. Pollack (1970), Near-infrared light scattering by terrestrial clouds, *J. Atmos. Sci.*, *27*, 265–281.

Horie, H., T. Iguchi, H. Hanado, H. Kuroiwa, H. Okamoto, and H. Kumagai (2000), Development of a 95-GHz airborne cloud profiling radar (SPIDER): Technical aspects, *IEICE Trans. Fundam. Electron. Commun. Comput. Sci.*, *38*(9), 2010–2020.

Kumagai, H., H. Horie, H. Kuroiwa, H. Okamoto, and S. Iwasaki (2000), Retrieval of cloud microphysics using 95-GHz cloud radar and microwave radiometer, *Proc. SPIE Int. Soc. Opt. Eng.*, *4152*, 364–371.

Moody, E. G., M. D. King, S. Platnick, C. B. Schaaf, and F. Gao (2005), Spatially complete global spectral surface albedos: Value-added datasets derived from Terra MODIS land products, *IEEE Trans. Geosci. Remote Sens.*, *43*, 144–158.

Nakajima, T., and M. D. King (1990), Determination of the optical thickness and effective particle radius of clouds from reflected solar radiation measurements. part I: Theory, *J. Atmos. Sci.*, *47*, 1878–1893.

Nakajima, T. Y., and T. Nakajima (1995), Wide area determination of cloud microphysical properties from NOAA AVHRR measurement for FIRE and ASTEX region, *J. Atmos. Sci.*, *52*, 4043–4059.

Nakajima, T., and M. Tanaka (1986), Matrix formulation for the transfer of solar radiation in a plane-parallel scattering atmosphere, *J. Quant. Spectrosc. Radiat. Transfer*, *35*, 13–21.

Nakajima, T., and M. Tanaka (1988), Algorithms for radiative intensity calculations in moderately thick atmospheres using a truncation approximation, *J. Quant. Spectrosc. Radiat. Transfer*, *40*, 51–69.

Okamoto, H., S. Iwasaki, M. Yasui, H. Horie, H. Kuroiwa, and H. Kumagai (2003), An algorithm for retrieval of cloud microphysics using 95-GHz cloud radar and lidar, *J. Geophys. Res.*, *108*(D7), 4226, doi:10.1029/2001JD001225.

Stamnes, K., S.-C. Tsay, W. Wiscombe, and K. Jayaweera (1988), Numerically stable algorithm for discrete-ordinate-method radiative transfer in multiple scattering and emitting layered media, *Appl. Opt.*, *27*, 2502–2509.

Twomey, S., and T. Cocks (1982), Spectral reflectance of clouds in the near-infrared: Comparison of measurements and calculations, *J. Meteorol. Soc. Jpn.*, *60*, 583–592.

Twomey, S., and K. J. Seton (1980), Inferences of gross microphysical properties of clouds from spectral reflectance measurements, *J. Atmos. Sci.*, *37*, 1065–1069.

A. Kamei, National Institute for Environmental Studies, 16-2 Onogawa, Tsukuba, Ibaraki 305-8505, Japan. (kamei.akihide@nies.go.jp)

N. Kikuchi, H. Kumagai, and H. Kuroiwa, National Institute of Information and Communications Technology, 4-2-1 Nukui-Kitamachi, Koganei, Tokyo 184-8795, Japan. (nobuhiro.kikuchi@nict.go.jp; kumagai@nict.go.jp; kuroiwa@nict.go.jp)

T. Nakajima, Center for Climate System Research, University of Tokyo, 5-1-5 Kashiwanoha, Kashiwa, Chiba 277-8568, Japan. (teruyuki@ccsr.u-tokyo.ac.jp)

T. Y. Nakajima, Department of Network and Computer Engineering, School of Engineering II, Tokai University, 2-28-4 Tomigaya, Shibuya, Tokyo 151-0063, Japan. (nkjm@yoyogi.ycc.u-tokai.ac.jp)

R. Nakamura, National Institute of Advanced Industrial Science and Technology, 1-1-1 Umezono, Tsukuba, Ibaraki 305-8568, Japan. (r.nakamura@aist.go.jp)